Chemical Engineering & Processing: Process Intensification 129 (2018) 77–83

Contents lists available at ScienceDirect

Chemical Engineering & Processing: Process Intensification

journal homepage: www.elsevier.com/locate/cep

Preparation of 3D graphene/iron oxides aerogels based on high-gravity intensified reactive precipitation and their applications for photo-Fenton reaction

Zhijian Zhao[a,b], Zhiyong Wang[a,b], Dan Wang[a,*], Jie-Xin Wang[a,b], Neil. R. Foster[a,c], Yuan Pu[b,*], Jian-Feng Chen[a,b]

[a] Research Center of the Ministry of Education for High Gravity Engineering and Technology, Beijing University of Chemical Technology, Beijing 100029, China
[b] State Key Laboratory of Organic-Inorganic Composites, Beijing University of Chemical Technology, Beijing 100029, China
[c] Department of Chemical Engineering, Curtin University, Perth, WA, 6845, Australia

ARTICLE INFO

Keywords:
High gravity technology
Iron oxides nanoparticles
Graphene aerogels
Intensified mixing
Photo-Fenton reaction

ABSTRACT

In this work, we reported the preparation of 3D graphene/iron oxides aerogels (IO/GA) by in situ growth of iron oxide nanoparticles (IO) on the graphene oxides in high gravity rotating packed bed (RPB) followed by freeze drying treatments. The RPB was used to intensify the mass transfer and mixing during the adsorption and nucleation process of IO, guaranteeing highly homogeneous reaction conditions to the reactants. Thereafter, the IO nanoparticles obtained in the RPB route (IO/GA-RPB) exhibited an average size of 6 nm with uniform size distribution. By contrast, the IO nanoparticles prepared from traditional stirred tank reactor (IO/GA-STR) showed much larger particle size (33 nm). The 3D structured IO/GA-RPB nanocomposites were demonstrated to be efficient heterogeneous photo-Fenton catalysts for the degradation of methyl-blue. The kinetic studies of the catalytic reaction systems in the temperature range of 293 K–323 K and pH value of 1–7 were performed. The reaction rate constants and apparent activation energy were determined. The related catalytic mechanism of the photo-Fenton reaction was investigated. The excellent catalytic efficiency of the 3D-foam-structured heterogeneous IO/GA-RPB catalyst, along with the knowledge of the kinetics data, make them promising for in scale-up applications of photo-Fenton reaction.

1. Introduction

Water pollution has recently been recognized as emerging environmental contaminants, especially in those developing countries [1]. Many approaches have been attempted to purify the contaminated water by separating the injurious components like sorption [2–4], membrane filtration [5], reverse osmosis, oxidation process [6,7] and so on [8,9]. Among them, oxidation process based on photo-Fenton reaction has been wildly used in water treatment due to its unique superiority of benign process, low cost, high efficiency and it is easy to regenerate [10,11]. Iron oxides (IO) nanoparticles have been emerging as promising heterogeneous catalysts for photo-Fenton degradation of organic dyes in sewage treatment due to its strong oxidation ability and easy recovery [12,13]. However, the IO nanoparticles can easily form aggregation in the liquid-phase reaction system, due to the strong anisotropic dipolar interactions between the IO particles [14,15], leading to significant decreasing in surface area and catalytic activity.

Graphene, a typical 2D carbon material, has shown potential as the support for nanocatalysts to avoid the particle aggregation and therefore to enhance the catalytic performance. To date, many kinds of metal/metal oxides nanomaterials including Pt, Ag, IO [16], Mn_3O_4 [17] have been loaded on the surface of graphene and its derives, which are extensively applied in electrode materials [18–20], catalysts [21–23], gas sensors and water purification [24–26]. However, the powder of 2D graphene based catalysts in liquid-solid or gas-liquid-solid multiphase reaction systems has some drawbacks such as aggregation and the bleeding of the graphene powders [27,28]. As alternative or additional solutions, 3D structured catalysts have many advantages over conventional powdered catalysts in terms of the transport characteristics and macro-kinetics of heterogeneous catalytic reactions [29]. In recent years, 3D structured graphene foam or aerogels have been well-developed as supports or even catalysts for various applications [30–32]. In particular, 3D graphene aerogels decorated with IO nanoparticles (IO/GA) have been reported to be promising adsorbents for water purification [33,34]. Nevertheless, the use of 3D IO/GA for photo-Fenton reaction has been rarely studied.

* Corresponding authors.
E-mail addresses: wangdan@mail.buct.edu.cn (D. Wang), puyuan@mail.buct.edu.cn (Y. Pu).

https://doi.org/10.1016/j.cep.2018.03.028
Received 9 February 2018; Received in revised form 22 March 2018; Accepted 27 March 2018
Available online 28 March 2018
0255-2701/

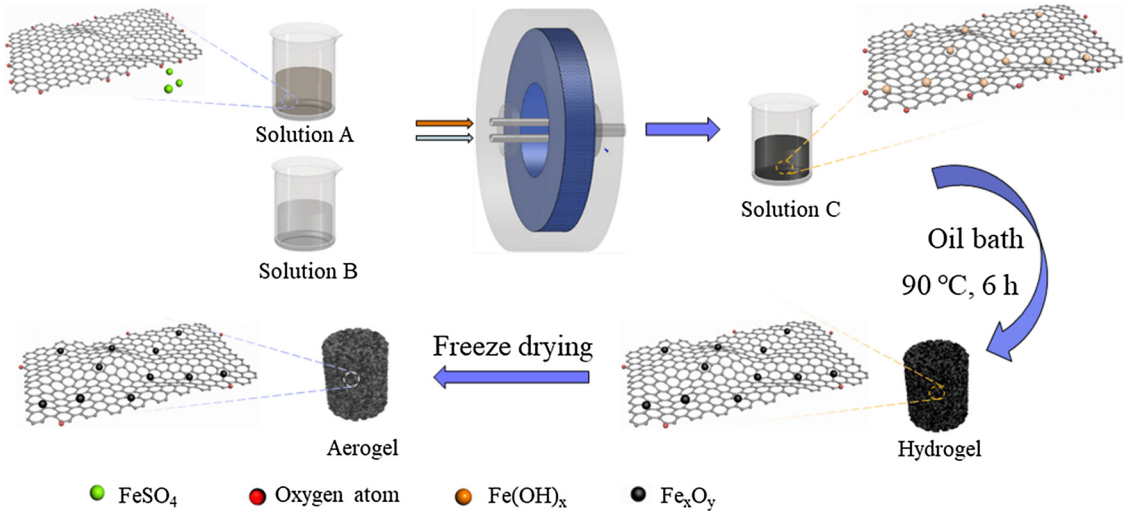

Fig. 1. Schematic diagram for the preparation of IO/GA based on high-gravity intensified reactive precipitation followed by freeze drying process.

As structured catalysts for photo-Fenton reaction, the size, distribution and loading density of IO nanoparticles deposited on the GA are critical for the catalytic performance [35]. However, there is still an obstacle for the preparation of uniform IO on graphene sheets. As for the formation of IO nanoparticles, the reaction parameters, such as temperature, stirring rate, precursor mixing have influence on the quality of final nanoparticles, while complete control of the reaction parameters is hard to achieve in traditional batch reactors, especially when large volumes of solution are involved. The high gravity rotating packed bed (RPB), a typical process intensification technology, has been demonstrated to be an efficient reactor for the preparation of nanoparticles [36,37]. In the RPB reactor, the aqueous reactants were spread or split into micro or nano droplets, threads or thin films, and the mass transfer and micromixing could be significantly intensified than those in conventional batch reactors. Lin et al. have demonstrated the continuous preparation of free-stand IO nanoparticles using a RPB rotating packed bed [38]. However, to the best of our knowledge, the high gravity RPB reactors have still not been applied in preparation of graphene supported IO nanocomposites.

In this work, we report the preparation of 3D graphene/iron oxides aerogels (IO/GA) by *in situ* growth of IO nanoparticles on the graphene oxides in high gravity RPB reactor followed by freeze drying treatments. The RPB is used to intensify the mass transfer and mixing during the adsorption and nucleation process of IO, guaranteeing highly homogeneous reaction conditions to the reactants. A variety of characterizations such as transmission electron microscopy (TEM), powder X-ray diffraction (XRD), Fourier transform infrared (FTIR) spectrophotometry and X-ray photoelectron spectroscopy measurements, are employed to investigate morphologies, crystal structures and surface properties of the IO/GA. Their catalytic performance as structured photo-Fenton reaction catalysts for the degradation of methyl-blue is investigated. The kinetic studies of the catalytic reaction systems in the temperature range of 293 K–323 K and pH value of 1–7 were studies and the related catalytic mechanism of the photo-Fenton reaction was analyzed.

2. Experimental section

2.1. Materials

Graphene oxides (GO) were produced by the modified Hummers methods [39]. $FeSO_4{\cdot}7H_2O$, ammonia and methylene blue were purchased from Sigma Aldrich. The reagents used as received without additional purification. Deionized water was used for all experiments.

2.2. Preparation of IO/GA

Typically, 280 mg of $FeSO_4{\cdot}7H_2O$ and 10 mL of GO aqueous suspension (4 mg mL^{-1}) were mixed in a cylindrical sampler vial, followed by ultrasonic treatment for 20 min to form well-dispersed solution (solution A). Another aqueous ammonia solution at pH value of 12 was prepared as solution B. Then, the two solutions were injected into a RPB reactor working at 2000 rpm and allowed to circulate in the RPB reactor for 30 min. The reaction products were then transferred into a flask and heated at 90 ℃ for 6 h without stirring. After that, the 3D monolith was taken out, washed with water, and freeze-dried (− 50 ℃, 48 h) into an aerogel for further use. The final product was denoted as IO/GA-RPB.

As a control experiment, a stirred tank reactor (STR) composed of a beaker and a stirrer, was used to mix the solution A and solution B. The final products were then obtained following the same heating and freeze drying process and denoted as IO/GA-STR.

2.3. Characterizations

The microstructures of the aerogel were imaged by a Hitachi HT7700 transmission electron microscope. The X-ray diffraction (XRD) analysis was performed on a Shimadzu XRD-6000 diffractometer. Fourier transform infrared (FTIR) spectra were measured by a Bruker Vector-70v FTIR spectrometer. X-ray photoelectron spectroscopy (XPS) measurements were performed on a VG Microtech ESCA 2000 instrument using a monochromic Al X-ray source. Raman spectra were collected on a Renishaw in via Raman spectrometer using a 633 nm wavelength laser as the excitation light. Thermogravimetric analyses (TGA) of samples were carried out using a VET ZSCh-SAT 449c instrument. The samples were tested with heating rate of 10 ℃ min^{-1} in nitrogen. The magnetic properties of the samples were investigated using a vibrating sample magnetometer (Physical Property Measurement System DynaCool, Quantum Design).

2.4. Catalytic performance of the IO/GA

The photocatalytic activity of the composite was evaluated in terms of the degradation of methylene blue (MB, 20 mg L^{-1}). The IO/GA was added to a sample vial containing 20 m L MB solution. Then 20 μL H_2O_2 (30 wt%) was added to the solution. A 500 W Xe lamp (Solar-500W, NBeT) was used as the simulated solar light source. Firstly, the solution was put into the darkness for 30 min to achieve the adsorption equilibrium, and then after the given time intervals exposed to the light, the

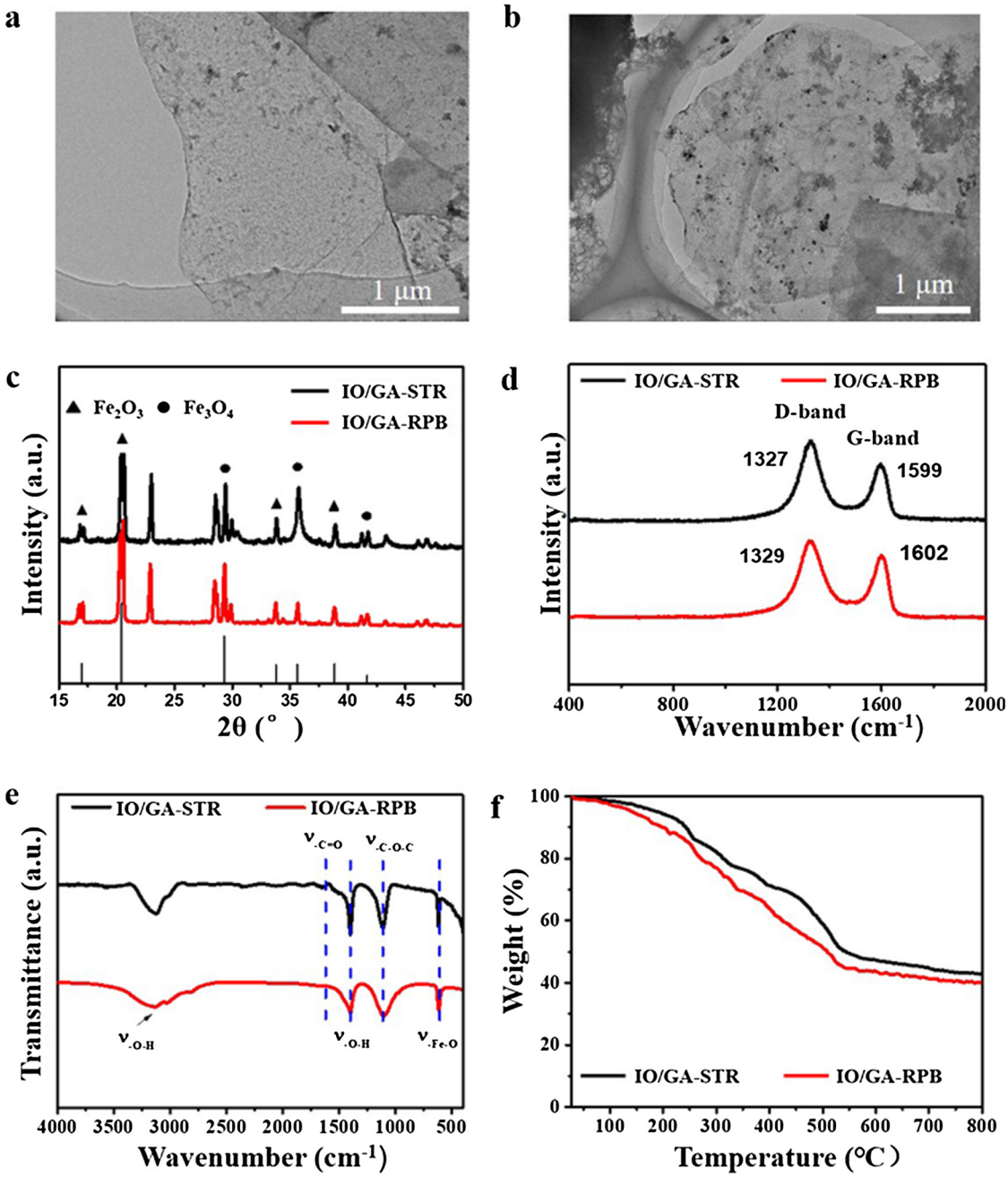

Fig. 2. (a, b) TEM images, (c) XRD patterns, (d) Raman spectra, (e) FTIR spectra and (f) TGA curves of IO/GA-RPB and IO/GA-STR.

samples were taken out at various time points and analyzed by a Shimadzu UV-2600 UV–vis scanning spectrophotometer.

3. Results and discussion

Fig. 1 shows the schematic diagram for the preparation of IO/GA-RPB based on high-gravity intensified reactive precipitation followed by freeze drying process. The aqueous solution A (mixture of GO and $FeSO_4$) and solution B (aqueous ammonia) were pumped into the RPB reactor. The nucleation of $Fe(OH)_x$ formed by precipitation and then crystallization. Since the heterogeneous nucleation has a lower activation energy barrier than homogeneous nucleation [40], the $Fe(OH)_x$ particles mainly occurred on the surface of GO. The RPB reactor guaranteed the highly homogeneous reaction conditions to the reactants for the precipitation process. During the heating of the primary reactants (solution C), the dispersed graphene oxides gradually assembled to a 3D hydrogel of graphene by the reduction of Fe^{2+}. At the same time, the $Fe(OH)_x$ particles were decomposed into IO and water. During the shrink of hydrogel, the solution became colorless, demonstrating that the iron ions were successfully anchored to the GA. Thereafter, freeze drying process is adopted to remove the water without damaging the 3D architecture, and the IO/GA-RPB was obtained. In this synthesis route, the $FeSO_4{\cdot}7H_2O$ served as both iron precursor and reductant, with the absence of organic reagent which is usually used for reducing graphene oxide to form a 3D framework. To investigate the effect of high-gravity RPB reactor on the preparation of IO/GA, we also synthesized the IO/GA following a previous reported route using batch STR to mix the solution A and solution B. After the same heating and freeze drying process, the IO/GA-STR was obtained for comparison.

Fig. 2a shows a typical TEM image of IO/GA-RPB, in which the IO/GA-RPB exhibited homogeneous distribution of IO nanoparticles on the

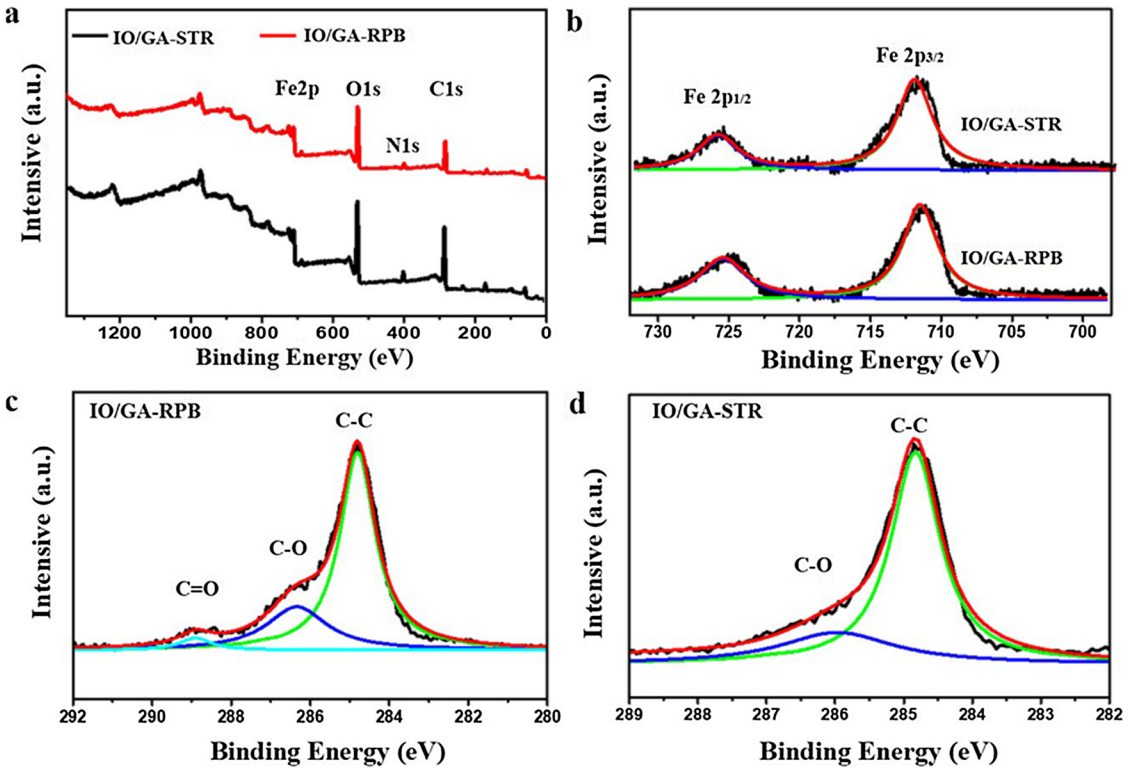

Fig. 3. (a) Survey scan and (b) high-resolution Fe2p XPS spectra of IO/GA-RPB and IO/GA-STR respectively. High-resolution C1s XPS spectrum of (c) IO/GA-RPB and (d) IO/GA-STR.

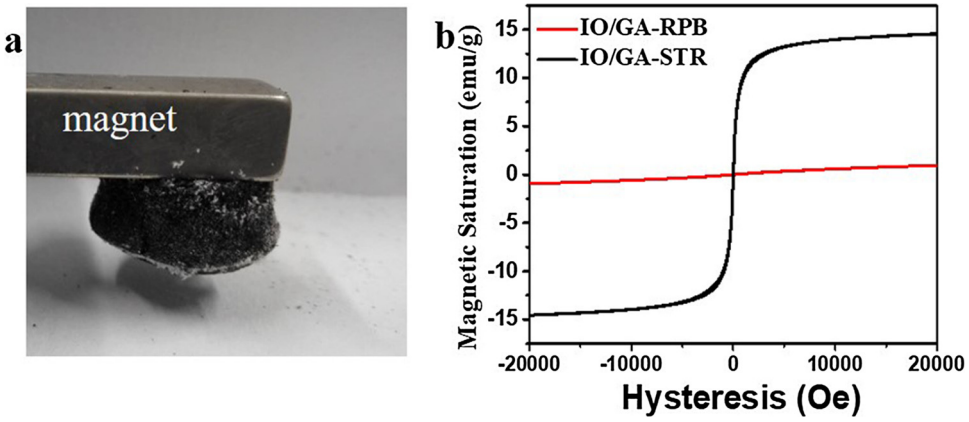

Fig. 4. (a) Photograph of the magnetic property of the aerogel; (b) Room-temperature hysteresis curves of the two aerogel.

surface of graphene. The average size of the IO nanoparticles was determined to be 6 nm according to the high-resolution TEM image (Fig. S1). By contrast, the IO nanoparticles in IO/GA-STR showed broad size distribution, with an average size of 30 nm (Fig. 2b). These results demonstrated the advantage of the process intensification by high gravity RPB reactor, which intensify the mass transfer and mixing during the adsorption and nucleation process of IO, guaranteeing highly homogeneous reaction conditions to the reactants. Therefore, the obtained nanoparticles by RPB route were much more uniform and smaller than those prepared in common STR. The XRD patterns in Fig. 2c illuminated the compositions of the 3D composites of IO/GA-RPB and IO/GA-STR. Both samples showed similar XRD patterns. The diffraction peaks were assigned to the mixture of the magnetic Fe_3O_4 (JCPDS No. 75-0033) and the orthorhombic phase α-FeOOH (JCPDS No. 29-0713), while the typical diffraction peak at around 23° was attributed to the supported reduced graphene oxide. And from the quantitative XRD analysis [41], the mass ratio of Fe_2O_3 and Fe_3O_4 is 3.

To further confirm the structural composition of the aerogel, Raman spectra measurements were performed. As shown in Fig. 2d, the ratio of the D band and G band (I_D/I_G) for the IO/GA-STR and IO/GA-RPB is 1.42 and 1.24. Both D band and G band exhibited slight shifts, which was attributed to the enhanced charge transfer between graphene sheets and IO nanoparticles [19]. The FTIR spectra of IO/GA-RPB and IO/GA-STR showed similar trends and characteristic bands (Fig. 2e). The peaks at 3215 cm^{-1} and 1423 cm^{-1} were attributed to the −COOH stretching vibrations [47]. The peak at 1713 cm^{-1} referred to the C=O (carboxyl) stretching vibrations and the absorption band at 1122 cm^{-1} related to the epoxy C−O stretching vibrations. The characteristic bending vibrations of Fe−OH and Fe−O were observed at 892 cm^{-1} and 544 cm^{-1} respectively [20]. The TGA curves of IO/GA-RPB and IO/GA-STR also exhibited similar drops in the temperature range of 25–800 ℃ in nitrogen. The initial drop below 100 ℃ is due to the water loss from the aerogel and the drop after that is attributed to the loss of oxygen-containing functional group like epoxied, carboxyl, and the

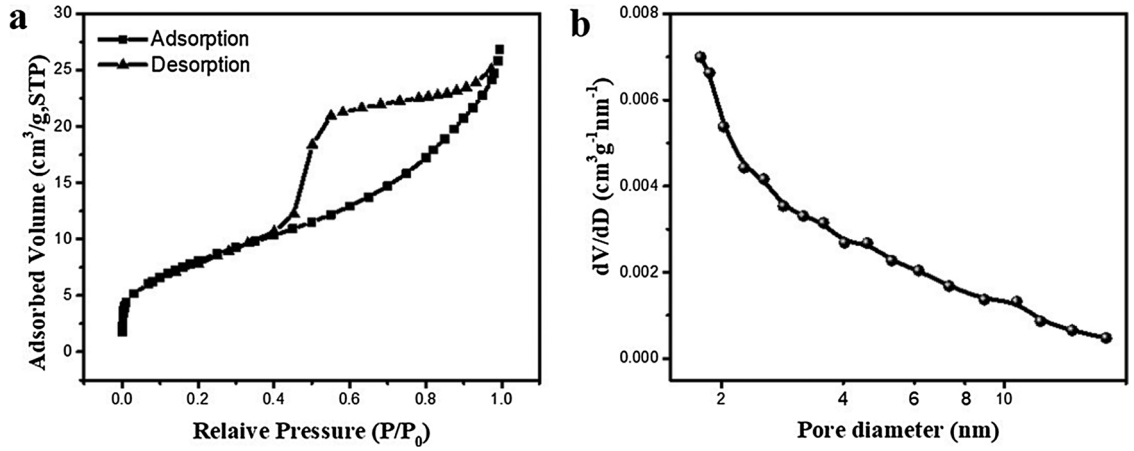

Fig. 5. (a) N_2 adsorption/desorption isotherms; (b) pore size distribution of IO/GA-RPB.

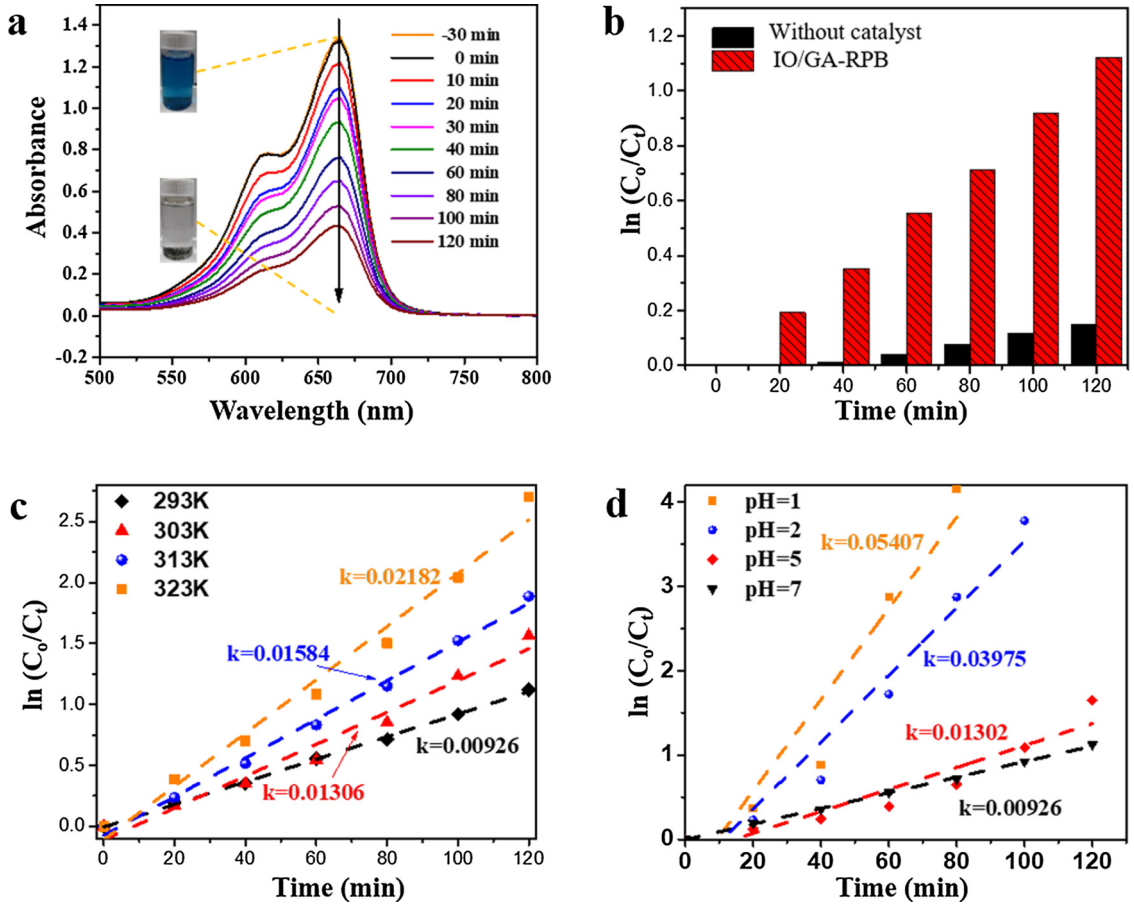

Fig. 6. (a) Degradation of MB recorded of photo-Fenton reaction by UV–vis scanning spectrophotometer; (b) Solar-driven degradation of methyl-blue (20 mL MB, 20 mg L^{-1}) under different reaction systems; (c) Solar-driven degradation of MB on IO/GA-RPB (20 μL, H_2O_2, 30 wt%) under different reaction temperatures; (d) The photo-Fenton reaction of IO/GA-RPB with different pH (the pH is adjusted by adding of 1 M HCl).

hydroxyl [42].

The atomic valence states of the 3D GA were also investigated by XPS and the results were shown in Fig. 3. The complete survey spectrum (Fig. 3a) showed the presence of C1s, O1s, N1s and Fe2p peaks, in which the doping of N (4.71% of atomic percentage) can promote the catalytic performance. The iron portion for IO/GA-RPB (3.85%) is larger than that of IO/GA-STR (2.85%), suggesting the higher IO loading density in GA by using RPB route than that using STR route. In the high-resolutions XPS spectrum of Fe2p, two obvious peaks observed at 711.1 eV and 724.7 eV were assigned to Fe $2p_{3/2}$ and Fe $2p_{1/2}$, which also verified the formation of IO [43]. The C1s XPS spectrum of IO/GA-RPB in Fig. 3c demonstrated the presence of carbon bond of graphite sp^2 C (284.75 eV), C—O (286.37 eV) and C═O (288.90 eV). The weak peaks of C═O and C—O confirmed the reduction of graphene oxide, which agreed well with the Raman spectra results (Fig. 2d). One should be payed intention is that IO/GA-STR showed than a higher degree of reduction in IO/GA-RPB, for the C═O peak disappears, and C—O peak is weaker, we believe that is the aggregate between graphene layers in IO/GA-RPB which cause the lower reduction degree. When the RPB system realize the nanoparticles with superfine size, it is inevitably to

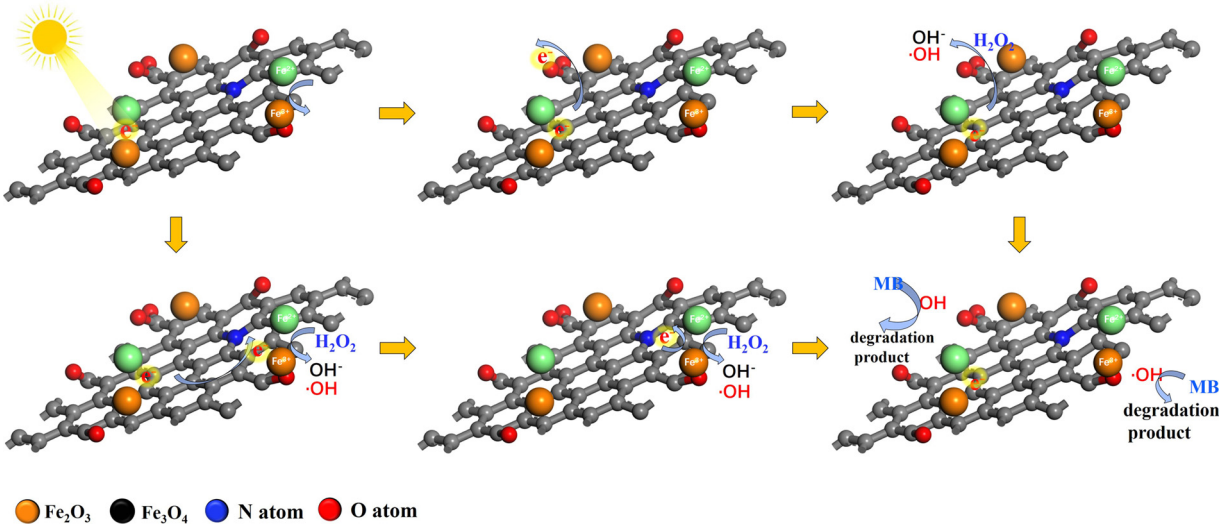

Fig. 7. Proposed catalytic mechanism for IO/GA in the photo-Fenton reaction.

cause the aggregate between layers for the lacking of obstruction.

Magnetic hysteresis curves of IO/GA-RPB and IO/GA-STR were measured to investigate the magnetic properties. As the results shown in Fig. 4 and Fig. S2, both the two samples showed superparamagnetic properties. The saturation magnetization (M_s) of IO/GA-STR is 14.5 emu g^{-1}, which is much lower than that of bulk magnetite Fe_3O_4 (92 emu g^{-1}). The lower density of magnetization value possibly have connection with the presence of graphene sheets and the lower density of magnetic components [44], but it is strong enough to be manipulated under low magnetic fields, shown as Fig. 4a. As for the IO/GA-RPB, the aerogel still did not reach its saturation state and showed at a very low value even the magnetic field was up to 20,000 Oe. This phenomenon was attributed to the ultrasmall particle size of IO in the IO/GA-RPB [45].

The Brunauer-Emmett-Teller (BET) specific surface area and porous structure characteristics of the IO/GA-RPB aerogel were investigated by nitrogen isothermal adsorption. The BET surface area of IO/GA-RPB was measured to be 29.43 $m^2 g^{-1}$. The nitrogen adsorption/desorption isotherms and the pore size distributions were shown in Fig. 5, which illustrated the mesoporous IO/GA-RPB with the pore size distributions in 2–10 nm. The pore volume gets from the Barret-Joyner-Halenda (BJH) method is 0.0372 $cm^3 g^{-1}$. The obtained composite with porous structure of mesoporous implied the hybrid material could have a great potential application in catalytic reactions.

It has been proved that the ferrous ions and H_2O_2 based photo-Fenton reaction is an effective technology in wastewater treatment, some reports have also demonstrated that the IO/GA are very promising as catalysts for photo-Fenton reaction [12,22]. In this work, the catalytic performance of IO/GA-RPB for solar-driven Fenton reactions under various conditions were measured by monitoring the change in optical absorption of a methyl-blue solution (MB, 20 mg L^{-1}, Fig. 6a). When excess H_2O_2 was used, the catalytic decomposition of MB by IO/GA in photo-Fenton reaction followed a pseudo-first-order kinetic (Fig. S3). On the basis of first-order reaction kinetics, the overall kinetics of MB decomposition showed as follow:

$$\frac{-dc_{MB}}{dt} = k_1 c_{MB} \quad (1)$$

$$\ln\frac{c_t}{c_0} = -k_1 t \quad (2)$$

where c_{MB} is the molar concentration of MB, k_1 is the decomposition rate constant at the specific temperature, and t is the reaction time. c_0 and c_t are the concentration of MB at the time of 0 and t.

Fig. 6b shows the extraordinary catalytic activity of IO/GA-RPB. It has been verified that GO can enhance catalytic performance of IO by transferring electrons to maintain the active Fe^{2+} sites and providing the H_2O_2 activation sites by the π-system of graphene oxide [12,46]. So the decrease of nanoparticles size can enhance the conjugation between IO and graphene to make the performance of graphene sheet get a further promotion. Therefore, IO/GA-RPB shows a higher catalyst activity than IO/GA-STR by 5.9% (Fig. S4). These results confirm that RPB is an advantageous technology in fulfilling the potential of IO/GA catalysts. To investigate the influence of temperature and pH on IO/GA-RPB, the reaction solution is adjusted to the desired pH from 1 to 7 by adding HCl and the temperature is set between 293 K–323 K. Fig. 6c showed that the catalytic performance was enhanced as the temperature increasing. Using the Arrhenius equation, the apparent activation energy (E_a) for degradation of MB over IO/GA-RPB was calculated to be 21.75 kJ mol^{-1} (Table S1 and Fig. S5). Table S2 shows that the apparent activation energy of composite prepared in this work is superior to some materials reported. Fig. 6d shows the degradation rate of MB rises with the increase of acidity, which can get explanation by the Eq. (3), in which the H^+ can consume OH- to promote process of reaction.

$$Fe^{2+} + H_2O_2 = Fe^{3+} + OH^- + OH\cdot \quad (3)$$

To explore the proposed catalytic mechanism of IO/GA, the GA without IO nanoparticles were prepared for comparison. The intrinsic GA showed almost the same catalytic activity as the system without catalyst, indicating no catalytic activity towards photo-Fenton reaction (Fig. S6). Therefore, the significant catalytic performance of IO/GA-RPB was attributed to the combined action of IO nanoparticles and GA. Fig. 7 showed the proposed catalytic mechanism for the IO/GA in photo-Fenton reaction. Firstly, the IO produces photogenerated electrons, and the graphene could suppress the recombination of the photogenerated electron-hole pairs [16]. Then the photogenerated electrons conduct to give the Fe^{3+}/Fe^{2+} cycle reaction which could reduce H_2O_2 to strong oxidizing ·OH radical. The MB molecule was then decomposed to H_2O and CO_2 by the function of the ·OH. That is, the IO particles on the surface of graphene provide the photogenerated electron to activate the catalytic reaction, and the catalytic performance get promoted owing to the excellent conductivity, so the nanoparticles with smaller size can enhance the conjugation between IO and graphene to accelerate the conduct of photogenerated electron.

4. Conclusions

In conclusion, we reported the preparation of 3D structured IO/GA by *in situ* growth of IO nanoparticles on the graphene oxides based on

high gravity intensified reactive precipitation of IO nanoparticles. Due to the intensified mass transfer and mixing during the adsorption and nucleation process of IO by RPB reactor, which realized highly homogeneous reaction conditions to the reactants, the IO nanoparticles obtained in IO/GA-RPB exhibited uniform distribution and ultrasmall average size (6 nm). The catalytic performance of IO/GA-RPB as structured photo-Fenton reaction catalysts for the degradation of methyl-blue was investigated and the kinetic knowledge of the catalytic reaction systems in the temperature range of 293 K–323 K and pH value of 1–7 were obtained, making them promising for in scale-up applications of photo-Fenton reaction.

Acknowledgments

We are grateful for financial support from the National Key Research and Development Program of China (2017YFA0206801), the National Natural Science Foundation of China (21620102007 and 21622601), the Fundamental Research Funds for the Central Universities of China (BUCTRC201601), and the “111” project of China (B14004).

Appendix A. Supplementary data

Supplementary data associated with this article can be found, in the online version, at https://doi.org/10.1016/j.cep.2018.03.028.

References

[1] Y. Li, R. Zhang, X. Tian, C. Yang, Z. Zhou, Facile synthesis of Fe_3O_4, nanoparticles decorated on 3D graphene aerogels as broad-spectrum sorbents for water treatment, Appl. Surf. Sci. 369 (2016) 11–18.
[2] X. Ruan, Y. Chen, H. Chen, G. Qian, R.L. Frost, Sorption behavior of methyl orange from aqueous solution on organic matter and reduced graphene oxides modified Ni–Cr layered double hydroxides, Chem. Eng. J. 297 (2016) 295–303.
[3] S. Gadipelli, X.G. Zheng, Graphene-based materials: synthesis and gas sorption, storage and separation, Prog. Mater. Sci. 69 (2015) 1–60.
[4] A. Subrati, S. Mondal, M. Ali, A. Alhindi, R. Ghazi, A. Abdala, D. Reinalda, S. Alhassan, Developing hydrophobic graphene foam for oil spill cleanup, Ind. Eng. Chem. Res. 56 (2017) 6945–6951.
[5] G.D. Kang, Y.M. Cao, Application and modification of poly (vinylidene fluoride) (PVDF) membranes-a review, J. Membr. Sci. 463 (2014) 145–165.
[6] V.K. Gupta, T. Eren, N. Atar, M.L. Yola, C. Parlak, $CoFe_2O_4$@TiO_2 decorated reduced graphene oxide nanocomposite for photocatalytic degradation of chlorpyrifos, J. Mol. Liq. 208 (2015) 122–129.
[7] T.A. Saleh, A. Sarı, M. Tuzen, Effective adsorption of antimony(III) from aqueous solutions by polyamide-graphene composite as a novel adsorbent, Chem. Eng. J. 307 (2016) 230–238.
[8] S. Jamil, S. Jeong, S. Vigneswaran, Application of pressure assisted forward osmosis for water purification and reuse of reverse osmosis concentrate from a water reclamation plant, Sep. Purif. Technol. 171 (2016) 182–190.
[9] X. Fan, G. Jiao, W. Zhao, P. Jin, X. Li, Magnetic IO-graphene composites as targeted drug nanocarriers for pH-activated release, Nanoscale 5 (2013) 1143–1152.
[10] P. Roonasi, A.Y. Nezhad, A comparative study of a series of ferrite nanoparticles as heterogeneous catalysts for phenol removal at neutral pH, Mater. Chem. Phys. 172 (2016) 143–149.
[11] J. Liu, D. Wang, M. Wang, D. Kong, Y. Zhang, J.-F. Chen, L. Dai, Uniform two-dimensional Co_3O_4 porous sheets: facile synthesis and enhanced photocatalytic performance, Chem. Eng. Technol. 39 (2016) 891–898.
[12] B. Qiu, M. Xing, J. Zhang, Stöber-like method to synthesize ultralight, porous, stretchable Fe_2O_3/graphene aerogels for excellent performance in photo-Fenton reaction and electrochemical capacitors, J. Mater. Chem. A 3 (2015) 12820–12827.
[13] N.A. Zubir, C. Yacou, J. Motuzas, X. Zhang, X.S. Zhao, J.D. Costa, The sacrificial role of graphene oxide in stabilising a Fenton-like catalyst GO-IO, Chem. Commun. 51 (2015) 9291–9293.
[14] J. Deng, X. Wen, Q. Wang, Solvothermal in situ synthesis of Fe_3O_4-multi-walled carbon nanotubes with enhanced heterogeneous Fenton-like activity, Mater. Res. Bull. 47 (2012) 3369–3376.
[15] A. Prakash, S. Chandra, D. Bahadur, Structural, magnetic, and textural properties of iron oxide-reduced graphene oxide hybrids and their use for the electrochemical detection of chromium, Carbon 50 (2012) 4209–4219.
[16] B. Liu, L. Tian, R. Wang, J. Yang, R. Guan, X. Chen, Pyrrolic-N-doped graphene oxide/Fe_2O_3 mesocrystal nanocomposite: efficient charge transfer and enhanced photo-Fenton catalytic activity, Appl. Surf. Sci. 422 (2017) 607–615.
[17] Y. Li, J. Qu, F. Gao, S. Lv, L. Shi, C. He, J. Sun, In situ fabrication of Mn_3O_4, decorated graphene oxide as a synergistic catalyst for degradation of methylene blue, Appl. Catal. B 162 (2015) 268–274.
[18] Y. Dou, J. Xu, B. Ruan, Q. Liu, Y. Pan, Z. Sun, S. Dou, Atomic layer-by-layer Co_3O_4/graphene composite for high performance lithium-ion batteries, Adv. Energy Mater. 6 (2016) 1501835.
[19] C. Ban, Z. Wu, D.T. Gillaspie, L. Chen, L. Yan, J.L. Blackburn, A.C. Dillon, Nanostructured IO/SWNT electrode: binder-free and high-rate Li-ion anode, Adv. Mater. 22 (2010) 145–149.
[20] S. Ni, X. Wang, G. Zhou, F. Yang, J. Wang, Q. Wang, D. He, Hydrothermal synthesis of Fe_3O_4, nanoparticles and its application in lithium ion battery, Mater. Lett. 63 (2009) 2701–2703.
[21] Z. Wang, R. Su, D. Wang, J. Shi, J.-X. Wang, Y. Pu, J.-F. Chen, Sulfurized graphene as efficient metal-free catalysts for reduction of 4nitrophenol to 4-aminophenol, Ind. Eng. Chem. Res. 56 (2017) 13610–13617.
[22] M. Royvaran, A. Taheri-Kafrani, A.L. Isfahani, S. Mohammadi, Functionalized superparamagnetic graphene oxide nanosheet in enzyme engineering: a highly dispersive, stable and robust biocatalyst, Chem. Eng. J. 288 (2016) 414–422.
[23] Z. Wang, Y. Pu, D. Wang, J. Shi, J.-X. Wang, J.-F. Chen, 3D-foam-structured nitrogen-doped graphene-Ni catalyst for highly efficient nitrobenzene reduction, AIChE J. 64 (2018) 1330–1338.
[24] J. Li, S. Zhao, X. Zeng, W. Huang, Z. Gong, G. Zhang, R. Sun, C.-P. Wong, Highly stretchable and sensitive strain sensor based on facilely prepared three-dimensional graphene foam composite, ACS Appl. Mater. Interfaces 8 (2016) 18954–18961.
[25] T. Esfandiyari, N. Nasirizadeh, M. Dehghani, M.H. Ehrampoosh, Graphene oxide based carbon composite as adsorbent for Hg removal: preparation, characterization, kinetics and isotherm studies, Chin. J. Chem. Eng. 25 (2017) 1170–1175.
[26] E. Pervaiz, V. Msa, Z. Bingxue, C. Yin, M. Yang, Nitrogen doped RGO-Co_3O_4 nanograin cookies: highly porous and robust catalyst for removing nitrophenol from waste water, Nanotechnology 28 (2017) 385703.
[27] R. Tschentscher, T.A. Nijhuis, J. Schaaf, B.M. Kuster, J.C. Schouten, Gas-liquid mass transfer in rotating solid foam reactors, Chem. Eng. Sci. 65 (2010) 472–479.
[28] G.-W. Chu, Y.-J. Song, W.-J. Zhang, Y. Luo, H.-K. Zou, Y. Xiang, J.-F. Chen, Micromixing efficiency enhancement in a rotating packed bed reactor with surface-modified nickel foam packing, Ind. Eng. Chem. Res. 54 (2015) 1697–1702.
[29] P. Marın, M.G. Hevia, S. Ordonez, F. Dıez, Combustion of methane lean mixtures in reverse flow reactors: comparison between packed and structured catalyst beds, Catal. Today 105 (2005) 701–708.
[30] S.T. Mitchell, N. Frese, A. Gölzhäuser, A. Bowers, K. Sattler, Ultralight carbon nanofoam from naphtalene-mediated hydrothermal sucrose carbonization, Carbon 95 (2015) 434–441.
[31] A. Beitollahi, M.S. Sheikhaleslami, A novel approach for development of graphene structure in mesoporous carbon of high specific surface area, Carbon 107 (2016) 440–447.
[32] H.M. Hegab, L. Zou, Graphene oxide-assisted membranes: fabrication and potential applications in desalination and water purification, J. Membr. Sci. 484 (2015) 95–106.
[33] X. Xu, H. Li, Q. Zhang, H. Zhang, H. Hu, Z. Zhao, J. Li, J. Li, Y. Qiao, Y. Gogotsi, Self-Sensing, ultralight, and conductive 3D graphene/iron oxide aerogel elastomer deformable in a magnetic field, ACS Nano 9 (2015) 3969–3977.
[34] H.-P. Cong, X.-C. Ren, P. Wang, S.-H. Yu, Macroscopic multifunctional graphene-based hydrogels and aerogels by a metal ion induced self-assembly process, ACS Nano 6 (2012) 2693–2703.
[35] R. Wang, C. Xu, M. Du, J. Sun, L. Gao, P. Zhang, H. Yao, C. Lin, Solvothermal-induced self-assembly of Fe_2O_3/GS aerogels for high Li-storage and excellent stability, Small 10 (2014) 2260–2269.
[36] J.-F. Chen, Y.-H. Wang, F. Guo, X.-M. Wang, C. Zheng, Synthesis of nanoparticles with novel technology: high-gravity reactive precipitation, Ind. Eng. Chem. Res. 39 (2000) 948–954.
[37] D.P. Rao, A. Bhowal, P.S. Goswami, Process intensification in rotating packed beds (HIGEE): an appraisal, Ind. Eng. Chem. Res. 43 (2004) 1150–1162.
[38] C.C. Lin, J.M. Ho, H.L. Hsieh, Feasibility of using a rotating packed bed in preparing Fe_3O_4, nanoparticles, Chem. Eng. J. 203 (2012) 88–94.
[39] J. Qian, D. Wang, F.-H. Cai, W. Xi, L. Peng, Z.-F. Zhu, H. He, M.-L. Hu, S. He, Observation of multiphoton-induced fluorescence from graphene oxide nanoparticles and applications in *in vivo* functional bioimaging, Angew. Chem. Int. Ed. 51 (2012) 10570–10575.
[40] J.S. Colton, N.P. Suh, The nucleation of microcellular thermoplastic foam with additives: part I: theoretical considerations, Polym. Eng. Sci. 27 (1987) 485–492.
[41] C.-Z. Liao, L. Zeng, K. Shih, Quantitative X-ray diffraction (QXRD) analysis for revealing thermal transformations of red mud, Chemosphere 131 (2015) 171–177.
[42] A. Subrati, S. Mondal, M. Ali, A. Alhindi, R. Ghazi, A. Abdala, D. Reinalda, S. Alhassan, Developing hydrophobic graphene foam for oil spill cleanup, Ind. Eng. Chem. Res. 56 (2017) 6945–6951.
[43] W. Chen, S. Li, C. Chen, L. Yan, Self-assembly and embedding of nanoparticles by in situ reduced graphene for preparation of a 3D graphene/nanoparticle aerogel, Adv. Mater. 23 (2011) 5679–5683.
[44] X. Fan, G. Jiao, W. Zhao, P. Jin, X. Li, Magnetic IO-graphene composites as targeted drug nanocarriers for pH-activated release, Nanoscale 5 (2013) 1143–1152.
[45] H. Iida, K. Takayanagi, T. Nakanishi, T. Osaka, Synthesis of IO nanoparticles with various sizes and magnetic properties by controlled hydrolysis, J. Colloid Interface Sci. 314 (2007) 274–280.
[46] J.-H. Yang, G. Sun, Y. Gao, H. Zhao, P. Tang, J. Tan, A.-H. Lu, D. Ma, Direct catalytic oxidation of benzene to phenol over metal-free graphene-based catalyst, Energy Environ. Sci. 6 (2013) 793–798.
[47] D. Wang, Z. Wang, Q. Zhan, Y. Pu, J.-X. Wang, N.F. Foster, L. Dai, Facile and scalable preparation of fluorescent carbon dots for multifunctional applications, Engineering 3 (2017) 402–408.